Dynamic hybrid coupling for elastic wave propagation: reflection and transmission analysis

S. Raorane [1], **T. Uhl** [2], **P. Packo** [2], **M. Leamy** [3]
[1] Academic Centre for Materials and Nanotechnology,
AGH University of Science and Technology, Poland
e-mail: **sraorane@agh.edu.pl**

[2] Department of Robotics and Mechatronics
AGH University of Science and Technology, Poland

[3] School of Mechanical Engineering,
Georgia Institute of Technology, USA

Abstract
The necessity of coupling different numerical techniques arises in many practical engineering problems. Among other, coupled models are common to the so-called multi-scale modeling problems, where at least two domains of different resolutions are combined in order to predict an object's behavior. For the case of dynamic coupling of different numerical methods, the phenomenon of artificial reflections - due to the difference in material properties, spatial discretization parameters and time steps used in the models - may arise. These reflections have significant impact on the accuracy of the results and hence study of reflection/transmission is an important aspect of numerical analysis. In this paper, the reflection and transmission properties of a dynamic hybrid coupling scheme for two dynamic transient models of elastic wave propagation, namely, the Local Interaction Simulation Approach (LISA) and Cellular Automata for Elastodynamics (CAFE), are analyzed and methods of minimizing these numerical errors are proposed.

1 Introduction

Multi-scale modeling is a fundamental concept in analyzing complex systems exhibiting several (at least two) levels of interest. The latter are related to various phenomena that are vital for the global response of the system, but occur at different temporal and spatial scales. A representative example of a physical system in structural dynamics - requiring a multi-scale analysis - is a structure with a crack. Phenomena occurring in the crack area, e.g. crack propagation, movement of crack faces, friction etc., require detailed analysis and - in the context of numerical modeling - high model resolutions in time and space. From the global perspective, however, such fine analysis applied to the whole structure is time-consuming and impractical. A trade-off between accuracy and computational burden can be achieved by employing two models of different resolutions - one for the crack and one of the remaining part of the domain - and coupling them seamlessly. Establishing proper coupling conditions for the interface between the two models - resulting in minimum errors - is the main challenge in multi-scale modeling. The complexity of the coupling depends on the types of models used, e.g. continuum/discrete, different approximation and/or interpolation schemes, or different spatial and/or temporal discretizations. The second factor influencing the complexity of the coupling is dynamics of the problem, e.g. static, quasi-static, modal, transient etc. While for static problems, the definition of coupling conditions is relatively easy and does not introduce significant overhead in computational time, dynamic systems are much more demanding. In the latter, in particular for dynamic transient analyses, coupling conditions need to ensure equilibrium of dynamic forces at each time step.

There are three major challenges of multi-scale modeling which need to be addressed in order to achieve

stable and accurate simulation results. Firstly, the dynamic coupling of displacements and forces at different scales of space and time, maintaining their continuity at the interface, needs to be achieved. Secondly, analysis of stability of the coupling interface needs to be carried out, as individual stability conditions of the coupled models do not guarantee stability of the whole multi-scale model. Thirdly, the quality of the coupling needs to be evaluated and - if necessary - corrections to the multi-scale scheme introduced. As will be shown throughout the paper, for practical problems the dynamic transient coupling of different space and time scales introduces artificial reflections. Analyzing and minimizing these numerical errors is crucial to achieve a successful multi-scale model. Therefore, as a measure of the coupling quality, we propose the transmission and reflection properties of the interface. Namely, zero (artificial) reflections and perfect transmission at the interface between the two models, will be characteristic of an ideal coupling scheme.

Many studies have been performed to address the issue of artificial/numerical reflections at the interface of coupled models. Sharan [1] proposed a non-reflecting boundary condition for the coupled vibration of an infinite fluid domain and a deformable structure of arbitrary geometry. A method to establish a non-reflecting boundary condition applicable to atomistic, continuum and coupled multi-scale atomistic-continuum simulations was proposed in [2]. In [3] a time-dependent boundary condition, coupling an atomistic simulation system to linear surroundings, to minimize boundary reflection was proposed. Owing to the drawbacks of non-reflecting boundary conditions [4], Linkamp *et al.* [5] proposed a non-reflecting coupling method for 1-D finite volume and 1-D finite difference methods based on spectral error analysis. Xiao and Belytschko [6] proposed a bridging domain method for coupling continuum and molecular models, which avoid spurious wave reflections at the molecular/continuum interface without any additional filtering procedures. More recently, Giannakeas *et al.* [7] presented a systematic analysis regarding the appearance of spurious reflections and the underlying parameters that control the accurate transmission of incident pulses across the coupling interface/zone. They assessed three different coupling methodologies - coupling bond-based peridynamic grids with finite elements for solid structures - to evaluate the severity of spurious reflections generated. Despite deriving non-reflecting boundary conditions, employing different coupling strategies and analyzing artificial reflections - according to the authors' knowledge - none of the works report on derivation of reflection and transmission formulas for multi-scale numerical models and discuss them in the context of impedance mismatch. This approach, frequently adopted for continuous [8] and discrete [9] physical systems, is applied for analyzing numerical reflection at the interface of two coupled numerical models in this work.

This paper focuses on developing methods for analysis of reflection and transmission properties of a multi-scale scheme for two dynamic transient models of elastic wave propagation, namely, the Local Interaction Simulation Approach (LISA) [10, 11, 12] and Cellular Automata for Elastodynamics (CAFE) [13, 12]. A hybrid approach coupling these two methods is appealing because of CAFE's capability to allow non-uniform meshes – used e.g. for modeling crack vicinity - coupled to very efficient LISA's rectangular meshes for the regular part of the domain [12]. The formulation and stability analysis of this multi-scale scheme is briefly described in [14]. The proposed approach is capable of coupling different spatial discretization parameters and/or time steps in LISA and CAFE, and hence experiences reflections that affect accuracy of the results. In this paper, reflections arising owing to different discretization parameters in LISA and CAFE are thoroughly analyzed. Apart from this analysis, a compensation scheme - allowing for adjustment of model parameters and reducing the amount of artificial reflections, is proposed and discussed.

This paper is organized as follows. First, LISA and CAFE are briefly introduced and their numerical properties outlined. Next, the coupling scheme for combining LISA and CAFE into a multi-scale model is proposed. In order to analyze reflection, the concept of numerical impedance is introduced and individual impedances of LISA and CAFE are determined. Numerical impedance contrasts with usual impedance for continuous media as the former is affected by spatial discretization parameters. Next, based on the individual LISA and CAFE impedances, the impedances of the multi-scale scheme are determined. A mismatch between these impedances gives rise to reflections in the coupled model, therefore equations to predict reflection/transmission at the coupled interface are subsequently derived. These equations, capable of predicting reflections for any combination of material properties and/or spatial discretization parameters in the coupling scheme, are validated against results from numerical simulations. Lastly, a compensation scheme to minimize these artificial reflections is subsequently discussed.

2 Numerical methods

In this section the two dynamic transient models of elastic wave propagation, LISA and CAFE, used in the coupling scheme are introduced. LISA is a top-down approach based on finite differences while CAFE is a bottom-up approach based on cellular automata [13, 11, 12]. The coupling of these two methods paves path for the usage of non-uniform CAFE meshes combined with highly efficient LISA's rectangular meshes in a multi-scale framework. In order to distinguish between quantities related to the two methods, capitalized letters, A, B, U, K, and ΔX will refer to the LISA domain, and lower-case letters, a, b, c, u, k, and Δx - to the CAFE domain, throughout the paper.

2.1 1-D LISA model

In 1-D LISA model, we adopt the standard discretization of a 1-D domain into a set of nodes positioned and numbered as shown in Fig. 1a. Cells Ⓐ and Ⓑ - occupying space between nodes $n-1$ and n, and n and $n+1$, respectively - are assigned with material properties defined by Young's modulus E and mass density ρ. This regular grid of cells is used for discretization of the 1-D wave equation

$$\rho U_{,tt} = \sigma_{,x}\,, \tag{1}$$

where ρ is the density, σ is the stress tensor and U is the displacement. The indexes after commas denote differentiation with respect to that quantity. Discretizing Eq. (1) at node n requires evaluation of $\sigma_{,x}$ at node n, i.e. at the discontinuity of cells Ⓐ and Ⓑ which requires particular treatment. As Eq. (1) holds individually in each cell we have

$$\rho^{\text{Ⓐ}} U_{n-\delta,tt} = \sigma_{n-\delta,x}, \qquad \rho^{\text{Ⓑ}} U_{n+\delta,tt} = \sigma_{n+\delta,x}\,, \tag{2}$$

where δ is a small distance ($\delta \ll$ node spacing). In Eqs. (2), the stresses $\sigma_{n\mp\delta,x}$ can be evaluated since there is no discontinuity inside each cell, and are given by

$$\sigma_{n-\delta,x} = \frac{2E^{\text{Ⓐ}}}{\Delta X}\left(U_{n-\delta,x} - U_{n-\frac{1}{2},x}\right), \qquad \sigma_{n+\delta,x} = \frac{2E^{\text{Ⓑ}}}{\Delta X}\left(U_{n+\frac{1}{2},x} - U_{n+\delta,x}\right)\,, \tag{3}$$

where ΔX is the distance between two adjacent nodes and the first order Euler finite difference formulas have been adopted for stresses in the two cells. The first-order derivatives $U_{n\mp\delta,x}$ cannot be evaluated for the reasons outlined above, however they can be removed by imposing stress continuity conditions at n. Assuming δ is small and noting that the stress continuity implies

$$\sigma_{n-\delta} = \sigma_{n+\delta} \quad \Leftrightarrow \quad E^{\text{Ⓐ}} U_{n-\delta,x} = E^{\text{Ⓑ}} U_{n+\delta,x}\,, \tag{4}$$

adding Eqs. (2) and using (3) and (4) yields

$$\frac{\rho^{\text{Ⓐ}} + \rho^{\text{Ⓑ}}}{2} U_{,tt} = \frac{E^{\text{Ⓑ}}}{\Delta X^2}(U_{n+1} - U_n) - \frac{E^{\text{Ⓐ}}}{\Delta X^2}(U_n - U_{n-1})\,. \tag{5}$$

Applying the second-order central difference operator to the LHS of Eq. (5) recovers the original displacement iteration equation for the 1-D LISA method [15].

Equation (5) governs wave propagation in 1-D LISA model. Frequency-dependent dispersion characteristics of this numerical scheme for a uniform, homogeneous rod can be obtained by requiring $\rho^{\text{Ⓐ}} = \rho^{\text{Ⓑ}} = \rho_L$, $E^{\text{Ⓐ}} = E^{\text{Ⓑ}} = E_L$ and assuming time- and space-harmonic motion of the form $U_n = \bar{U}_n e^{\mathrm{i}(K\,n\,\Delta X - \omega t)}$,

$$\omega^2 \rho_L = \frac{2E_L}{\Delta X^2}\left(1 - \cos(K\Delta X)\right), \tag{6}$$

(a) (b)

Figure 1: Discretized LISA domain: (a) a standard arrangement of two cells, (b) analogous setup where the right cell is replaced by an impedance.

with K and ω being the wavenumber in the LISA domain and angular frequency, respectively. Detailed discussion on dispersion in numerical models can be found in [16].

2.2 1-D CAFE model

CAFE adopts different material distribution in space than LISA. Namely, three cells - with possibly different material properties - are employed to obtain the iteration equation for 1-D CAFE as shown in Fig. 2a. Elastic constants, $E^{a,b,c}$, and densities, $\rho^{a,b,c}$, are associated with cells - a, b and c - at nodes $n-1$, n and $n+1$, respectively. This setup of cells is used to solve the balance of momentum for the middle cell as

$$m_b \ddot{u}_n = \sum F = F_{Right} - F_{Left}\,, \tag{7}$$

where $m_b = \rho^b \Delta x\, A$ is the mass of cell b, A is the cross section of the rod, Δx is the cell length, and $\sum F$ represents the sum of forces acting on the middle cell. F_{Right} is the force acting on cell b by cell c and F_{Left} is the force acting on cell b by cell a. In terms of stresses, F_{Left} and F_{Right} are evaluated as

$$F_{Left} = \sigma_{Left} A, \qquad F_{Right} = \sigma_{Right} A\,, \tag{8}$$

where σ_{Left} and σ_{Right} are then determined using Hooke's law in each cell as

$$\sigma_{Left} = \left(\frac{E^a + E^b}{2}\right)\left(\frac{u_n - u_{n-1}}{\Delta x}\right), \qquad \sigma_{Right} = \left(\frac{E^b + E^b}{2}\right)\left(\frac{u_{n+1} - u_n}{\Delta x}\right). \tag{9}$$

Using Eqs. (9) and (8) in (7) gives

$$m_b \ddot{u}_n = \left(\frac{E^b + E^b}{2}\right)\frac{A}{\Delta x}(u_{n+1} - u_n) - \left(\frac{E^a + E^b}{2}\right)\frac{A}{\Delta x}(u_n - u_{n-1})\,. \tag{10}$$

Applying the second-order central difference operator to the LHS in Eq. (10) recovers the original displacement iteration equation for the 1-D CAFE method [13].

As before, frequency-dependent dispersion characteristics of CAFE for a uniform, homogeneous rod can be obtained by requiring $\rho^b = \rho_C$, $E^a = E^b = E^c = E_C$ and assuming time- and space-harmonic motion of the form $u_n = \bar{u}_n e^{\mathrm{i}(k n \Delta x - \omega t)}$,

$$\omega^2 \rho_C = \frac{2E_C}{\Delta x^2}\left(1 - \cos(k\Delta x)\right), \tag{11}$$

with k being the wavenumber in the CAFE model.

Figure 2: Discretized CAFE domain: (a) a standard arrangement of three cells, (b) analogous setup where the left cell is replaced by an impedance.

2.3 A multi-scale LISA-CAFE model

In this section we propose a method for dynamic coupling of LISA and CAFE in a single multi-scale model. The coupling strategy and the resulting iteration equation of the coupled model will be next investigated for artificial reflections at the interface. Cells arrangement for the proposed coupling scheme is shown in Fig. 3. The procedure relies on exchanging data between the models in each iteration - CAFE cell's displacements are applied to the LISA domain through prescribed displacement boundary condition, while reaction forces are computed from LISA and passed to the coupled CAFE cell through a force boundary condition.

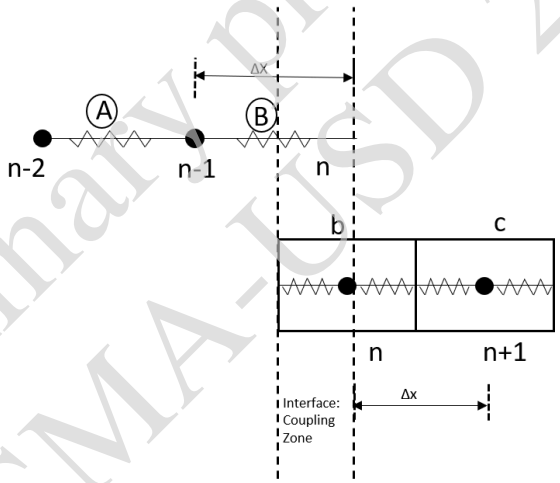

Figure 3: Cells' arrangement of the coupled model for LISA (top) and CAFE (bottom). The coupling zone is marked by dashed lines. Note the models overlap in the coupling zone.

The resulting iteration equation is obtained from (7) by replacing the left-hand side force acting on the cell, F_{Left}, by the reaction force from the LISA model, namely

$$-\omega^2 m_b u_n = \frac{\bar{E}A}{\Delta x} u_{n+1} - \left(\frac{\bar{E}A}{\Delta x} + \frac{E^{\textcircled{B}}A}{\Delta X}\right) u_n + \frac{E^{\textcircled{B}}A}{\Delta X} U_{n-1}\,, \tag{12}$$

where $2\bar{E} = E^b + E^c$ and A is the cross section of the rod. Equation (12) combines CAFE and LISA degrees of freedom and governs the dynamic equilibrium at the interface between the two models. Note that the time dependence of $e^{-\mathrm{i}\omega t}$ has been used in Eq. (12).

3 Complex impedance of a numerical scheme

Complex numerical impedance differs from its counterpart for continuous media [8, 9] and shares common features with its definition in discrete mass chains or crystals [9]. Specifically, the former depends on spatial discretization parameters along with material properties of the system. In this work, complex numerical impedances are derived in order to study artificial reflections arising at the interface of two coupled numerical models owing to numerical impedance mismatch. The impedance is defined as the ratio of force applied to the resulting velocity at a point

$$F = -Z\dot{u}\,, \tag{13}$$

where, F is the external force acting on the considered point, $\dot{u}$ is the velocity of the point, and Z is the impedance [9]. In the following sections we adopt the concept of impedance, Eq. (13), to derive complex impedances characteristic to two local numerical models, i.e. LISA and CAFE, and study artificial reflections at an interface of these two models. It will be shown that the respective numerical impedances can be obtained directly from the iteration formulas of the methods.

3.1 Complex impedance of the LISA model

For studying coupling of two different numerical schemes and to analyze numerical reflections it is instructive to look at the characteristic impedance of a model. As illustrated in Fig. 1b, impedance Z_L^R replaces the influence of cell Ⓑ on cell Ⓐ. The formula for Z_L^R can be obtained directly from Fig. 1b or from the iteration equation, Eq. (5). The latter approach will be shown here, as it is more general and applies also to more complex, asymmetric, cells. From Eqs. (13) and (5) it is clear that the impedance satisfies the following relation

$$\frac{Z_L^R \dot{U}_n}{A\,\Delta X} = -\frac{E^{\text{Ⓐ}}}{\Delta X^2}(U_n - U_{n-1}) - \frac{1}{2}\rho^{\text{Ⓐ}}\ddot{U}_n\,. \tag{14}$$

Note that half of the mass of the n^{th} node - residing in cell Ⓐ - has been included in Eq. (14). Using the space- and time-harmonic motion of the form $U_n = \bar{U}_n e^{\mathrm{i}(Kn\Delta X - \omega t)}$, and uniform material distribution, Eq. (14) becomes

$$\frac{\mathrm{i}\omega Z_L^R U_n}{A\,\Delta X} = \frac{E_L}{\Delta X^2}(1 - e^{-\mathrm{i}K\Delta X})U_n - \omega^2\frac{1}{2}\rho_L U_n\,. \tag{15}$$

The RHS of Eq. (15) can be further simplified by employing the dispersion relation, Eq. (6) and the numerical impedance at the right side of cell Ⓐ finally yields

$$Z_L^R = \frac{E_L A}{\Delta X \omega}\sin(K\Delta X)\,. \tag{16}$$

Following the same procedure, the numerical impedance at the left end of cell Ⓑ is found to be the same, i.e. $Z_L^L = Z_L^R = \frac{E_L A}{\Delta X\omega}\sin(K\Delta X)$. The real-valued numerical impedances at both ends, Z_L^R and Z_L^L, are a consequence of the symmetric mass distribution within the cells (Fig. 1). In contrast, an asymmetric cell - frequent in numerical models - will display a complex impedance. Such a case will be shown next for a numerical model that yields the same dispersion relation, but assumes different mass distribution than the LISA model.

3.2 Complex impedance of the CAFE model

Deriving impedance for CAFE is more natural since forces are explicitly present in the formulation. To determine the impedance on the left side of cell b (see Fig. 2b), we take $F_{Left} = -Z_C^L\dot{u}_n$. Then, Eq. (7)

becomes

$$m_b \ddot{u}_n = F_{Right} + Z_C^L \dot{u}_n, \tag{17}$$

which, using Eq. (10), becomes

$$\mathrm{i}\omega u_n Z_C^L = \left(\frac{E^b + E^c}{2}\right)\frac{A}{\Delta x}(u_{n+1} - u_n) + \omega^2 m_b u_n. \tag{18}$$

Assuming homogeneous material distribution, i.e. $E^b = E^c = E_C$, Eq. (18) further becomes

$$\mathrm{i}\omega Z_C^L = \frac{E_C A}{\Delta x}\left(e^{\mathrm{i}k\Delta x} - 1\right) + \omega^2 A \Delta x \rho_C. \tag{19}$$

Using the dispersion relation, Eq. (11), in Eq. (19), we get impedance on the left side of cell b

$$Z_C^L = \frac{E_C A}{\Delta x \omega}\sin(k\Delta x) - \mathrm{i}\frac{E_C A}{\Delta x \omega}(1 - \cos(k\Delta x))\,. \tag{20}$$

Following the same procedure, impedance at the right side of cell b is found to be the complex conjugate of Z_C^L, i.e. $Z_C^R = \frac{E_C A}{\Delta x \omega}\sin(k\Delta x) + \mathrm{i}\frac{E_C A}{\Delta x \omega}(1 - \cos(k\Delta x))$.

It can be observed that unlike in LISA, where the impedance is purely real, the impedance at either end of a CAFE cell is complex, which suggests that the mass distribution is asymmetric. In an asymmetric arrangement the mass is assumed to be either on the left side, or on the right side, of the cells depending on the impedance used.

4 Complex impedance of the interface cell

Analysis of the coupled scheme requires derivation of impedance of the LISA and CAFE parts of the model at the interface. Note that these may be different than those obtained in Sec. 3.1 and 3.2, depending on the mass-stiffness distribution within the cells. The latter depend on the employed coupling strategy. Next, we outline procedures for determining complex impedance formulas from the perspective of individual models, analogously to Sec. 3.

The coupled scheme, as shown in Fig. 3, involves a LISA cell at the left and a CAFE cell at the right of the interface. Because the CAFE node is assumed the master node in the coupling procedure (i.e. its displacement is passed to LISA), the CAFE left-end impedance is the same as derived in Eq. (20) and shown in Fig. 4b, while the LISA cell becomes asymmetric, as shown in Fig. 4a. For an asymmetric cell, the impedance is no longer real (see Eq. 16) but becomes complex.

(a) (b)

Figure 4: Arrangement of the LISA, (a), and CAFE, (b), parts of the coupled model.

In order to derive the impedance formula for the asymmetric cell of Fig. 4a, we use the LISA iteration equation, (5) with uniform material distribution

$$\frac{Z_L^L \dot{U}_{n-1}}{A\,\Delta X} = -\frac{E_L}{\Delta X^2}(U_{n-1} - U_{n-2}) - \rho_L \ddot{U}_{n-1}\,, \tag{21}$$

where ρ_L is the mass density at node $n-1$ (note the $1/2$ factor in Eq. (14)). Note that full mass of the $n-1^{th}$ node - residing in the asymmetric LISA cell adjacent to the interface - has been used in Eq. (21) unlike in 3.1 where the mass distribution is symmetric. Using the space- and time-harmonic motion of the form $U_n = \bar{U}_n e^{\mathrm{i}(K\,n\,\Delta X - \omega\,t)}$, Eq. (21) becomes

$$\frac{\mathrm{i}\omega Z_L^L U_{n-1}}{A\,\Delta X} = \frac{E_L}{\Delta X 2}(1 - e^{-\mathrm{i}K\Delta X})U_{n-1} - \omega^2 \rho_L U_{n-1}\,. \tag{22}$$

Using the dispersion relation Eq. (6), the complex impedance for the asymmetric LISA cell adjacent to the interface yields

$$Z_L^L = \frac{E_L A}{\Delta X \omega}\sin(K\Delta X) + \mathrm{i}\frac{E_L A}{\Delta X \omega}(1 - \cos(K\Delta X))\,. \tag{23}$$

Combination of cells from Figs. 4a and 4b, resembles the coupling node setup presented in Fig. 3. Consequently, the characteristic impedances of cells from Fig. 4a - Eq. (23) - and Fig. 4b - Eq. (20) - will be of interest to determine impedance mismatch and quantify numerical reflections.

5 Reflection and Transmission at the interface

The coupled multi-scale model outlined in Sec. 2.3 combines the LISA and CAFE domains via Eq. (12). The interface properties - and therefore possible artificial reflections - will depend on the individual models' and the coupling equations properties. The derivation of formulas for reflection and transmission coefficients for the interface follows a procedure similar to the continuous and discrete cases [9], i.e. employs the displacement and force continuity relations.

We assume the following grid functions for the wavefield before, $n < 0$, and after, $n > 0$, the interface

$$u_n = \begin{cases} Ie^{\mathrm{i}Kn\Delta X} + Re^{-\mathrm{i}Kn\Delta X} & \text{for } n < 0\,, \\ Te^{\mathrm{i}kn\Delta x} & \text{for } n > 0, \end{cases} \tag{24}$$

where I, R and T are (complex) amplitudes of the incident, reflected and transmitted waves, respectively. For $I = 1$, R and T become the reflection and transmission coefficients. At the interface, i.e. $n = 0$, $T = I + R$, as required by displacement continuity.

The force continuity at the interface is obtained from the coupling equation, Eq. (12), by noting that the forces on the right to the interface (i.e. $n > 0$, for the CAFE model), can be written as $\mathrm{i}\omega Z_C^L u_{T,0}$ (see Eq. (20)), while the forces on the left to the interface (i.e. $n < 0$, for the LISA domain), as $\mathrm{i}\omega\left(Z_L^L(I)u_{I,-1} + Z_L^L(R)u_{R,-1}\right)$ (see Eq. (23)). The latter sum relates to the two waves, incident and reflected, in the LISA domain and $u_{T,0}$, $u_{I,-1}$ and $u_{R,-1}$ are the displacements of the transmitted (at $n = 0$), incident and reflected (at $n = -1$) waves. The force equilibrium at the interface requires that

$$Z_C^L u_{T,0} = Z_L^L(I)u_{I,-1} + Z_L^L(R)u_{R,-1} = Z_L^L(I)e^{-\mathrm{i}K\Delta X}u_{I,0} + Z_L^L(R)e^{+\mathrm{i}K\Delta X}u_{R,0}. \tag{25}$$

Noting that $Z_L^L(I)e^{-\mathrm{i}K\Delta X} = Z_{0,L}^L(I)$ and $Z_L^L(R)e^{+\mathrm{i}K\Delta X} = Z_{0,L}^L(R)$ are impedances translated to the interface, using $T = I + R$ and taking $I = 1$, Eq. (25) can be used to determine the reflection coefficient

$$R = \frac{Z^L_{0,L}(I) - Z^L_C}{Z^L_C - Z^L_{0,L}(R)}, \tag{26}$$

where the amplitudes at the interface have been taken as $u_{T,0} = T$, $u_{I,0} = I$ and $u_{R,0} = R$. Equation (26) quantifies reflection of waves at the LISA/CAFE coupled interface. As the impedances - and in-turn the reflection coefficient - are functions of both spatial discretizaton lengths and material properties, LISA/CAFE models with the same material properties but different spatial discretization lengths will give rise to an impedance mismatch leading to artificial reflections. Please note that such artificial reflections are purely a numerical phenomenon and are characteristic of numerical errors.

The reflection coefficient computed using Eq. (26) is presented in Fig. 5 for a model with the same material properties in LISA and CAFE domains, but with different spatial discretization lengths, i.e. $\Delta x = 2\Delta X$. This choice would be common for a multi-scale analysis and illustrates that numerical reflections will occur at an interface of two nominally the same materials with different discretizations. The blue line shows reflection coefficient computed with Eq. (26). Clearly, R is non-zero indicating that waves will be reflected from the interface of the two models. At $\omega = 1$ - characteristic of the cut-off frequency for the CAFE model - the incident wave is fully reflected, i.e. $|R| = 1$.

We validate these results by a set of dynamic transient simulations. The model is composed of two parts, LISA and CAFE, long enough to avoid edge reflections. The wave excitation, at a given frequency, was provided by a narrowband wave packet with 200 sine periods shaped by half-Hann-windowing of the first and last 30 wave periods, retaining unit amplitude for the central part of the wavepacket. The wave was injected from the LISA side of the model (left) and was allowed to reach the interface and undergo reflection and transmission. After the reflected and transmitted waves were fully formed, the amplitude of the reflected wave was measured in the frequency domain. To determine the amplitude, the portion of the wave packet where the response was in-steady state was recorded and the Fast Fourier Transform (FFT) was applied to find its spectrum. The absolute value of the FFT at a selected frequency was taken as the reflected wave amplitude. The determined (measured) amplitude of the reflected wave was marked with squares and circles and superimposed on continuous lines (analytical solutions) in Fig. 5. Perfect agreement between the analytical and numerical simulations results can be observed.

Knowing the explicit relations governing reflection at the interface, Eq. (26), we attempt to minimize numerical reflections to achieve smooth and accurate coupling scheme. This minimization of artificial reflection is done using a compensation scheme, which will be discussed in the following section.

6 Compensation scheme

Artificial reflections affect the accuracy of numerical model results and their minimization is critical for developing reliable multi-scale schemes. In this section, a compensation scheme based on minimizing the impedance mismatch (Eq. (26)) is discussed. For minimizing R, different model parameters are tuned: Young's modulus, density and the spatial discretization length - all related to the CAFE domain. Although for a multi-scale model, dissimilar spatial discretizations are expected ($\Delta X \neq \Delta x$), compensation by adjusting Δx is shown in order to validate the proposed scheme. This naturally leads to the trivial condition $\Delta x = \Delta X$ in order to obtain $R = 0$.

Following Eq. (26), a simple approach for minimizing reflection can be proposed. Noting that the reflection, given by Eq. (26), depends on the Young's moduli, densities and the spatial discretization lengths, those parameters can be used to minimize R by requiring $R \to 0$. Various minimization techniques and frequency bands can be used. In what follows we restrict the analysis to the simplest single-frequency case, i.e. select a frequency and minimize R by tuning a single parameter E_C, ρ_C or Δx. Enforcing $R = 0$ (Eq. (26)), we get

$$Z^L_{0,L}(I) = Z^L_C\,. \tag{27}$$

Equation (27) is then solved in terms of Young's modulus of CAFE (E_C), density of CAFE (ρ_C), or spatial discretization length of CAFE (Δx) at every frequency to arrive at optimal model parameters. Note that Eq. (27) is complex, therefore real and imaginary parts need to be analyzed separately. Please note that for the trivial case of altering Δx, the optimal cell length will be the same for all frequencies and it will be equal to the spatial discretization length of LISA, ΔX. Results for all three compensation approaches are presented in Fig. 5.

It can be observed that the compensation results obtained by changing E_C and ρ_C are the same - a natural consequence of a single unique parameter in the model - the wave speed $V_C = \sqrt{E_C/\rho_C}$. It can be also observed that numerical reflections can be perfectly compensated for $\Delta x = \Delta X$, since the impedance mismatch between the LISA and CAFE domains - for the same material properties - arises only due to the difference in spatial discretization lengths in both these domains and vanishes for $\Delta x = \Delta X$.

Figure 5 shows that the proposed compensation scheme works also beyond the initial cut-off frequency ($\omega = 1$), and hence it can be used when the operating frequency is beyond the cut-off frequency to allow transmission and reduce reflections. As before, dynamic transient simulations were performed to validate the compensation results. Results of dynamic transient simulations are shown in Fig. 5 with markers (circles). Perfect agreement between the analytical and numerical simulations' results was observed.

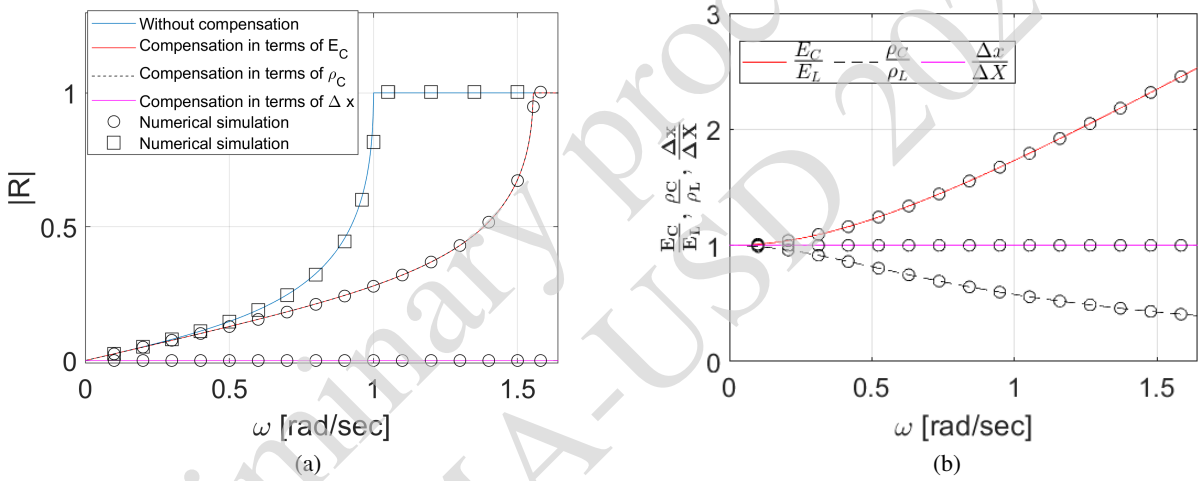

Figure 5: (a) Artificial reflections for the original and compensated schemes. (b) Ratios of compensated Young's moduli, densities and cell discretization lengths of CAFE to respective LISA counterparts. Markers indicate numerical simulations' results.

7 Conclusions

The analysis of reflection and transmission properties of a multi-scale scheme for two dynamic transient numerical models of elastic wave propagation, namely, the Local Interaction Simulation Approach and Cellular Automata for Elastodynamics has been reported. The LISA and CAFE numerical impedances for the dynamic coupling scheme have been derived and it was shown that unlike the usual impedance, numerical impedance is also affected by spatial discretization parameters. It was observed that for the multi-scale model the standard, asymmetric, arrangement of the CAFE cell is combined with an asymmetric arrangement of the LISA cell. Based on numerical impedances of the LISA, CAFE and the interface of the coupling scheme - all in the asymmetric arrangements - equations for predicting artificial reflections at the interface for any combination of material properties and/or spatial discretization lengths have been proposed. The scenario of equal material properties with dissimilar spatial discretization lengths in LISA and CAFE domains - giving rise to artificial reflections due to numerical impedance mismatch - was studied. It was concluded that artificial reflections, which are purely a numerical phenomenon, and affect the accuracy of results, are bound to

take place when cell discretizaton lengths are different, even when the material properties are the same. It has been found that a full reflection occurs for frequencies beyond the cut-off frequency of the second model.

To minimize the aforementioned artificial reflections, a compensation scheme, based on minimizing the impedance mismatch at a single frequency (Eq. (27)), has been reported in this paper. The impedance mismatch, and in turn the artificial reflections, can be minimized by altering either the elastic constants or numerical parameters of the models. The proposed technique can be also employed for extending the frequency range of model operation by effectively shifting the cut-off frequency.

Acknowledgements

This project has received funding from the European Union's Horizon 2020 research and innovation programme under the Marie Skłodowska-Curie grant agreement No. 764547. The third author acknowledges support from the National Science Centre through the OPUS project no. 2018/31/B/ST8/00753.

References

[1] S. Sharan, "A non-reflecting boundary in fluid-structure interaction," *Computers & structures*, vol. 26, no. 5, pp. 841–846, 1987.

[2] H. S. Park, E. G. Karpov, and W. K. Liu, "Non-reflecting boundary conditions for atomistic, continuum and coupled atomistic/continuum simulations," *International Journal for Numerical Methods in Engineering*, vol. 64, no. 2, pp. 237–259, 2005.

[3] W. Cai, M. de Koning, V. V. Bulatov, and S. Yip, "Minimizing boundary reflections in coupled-domain simulations," *Physical Review Letters*, vol. 85, no. 15, p. 3213, 2000.

[4] D. Givoli, "Non-reflecting boundary conditions," *Journal of computational physics*, vol. 94, no. 1, pp. 1–29, 1991.

[5] A. Linkamp, C. Deimel, A. Bruemmer, and R. Skoda, "Non-reflecting coupling method for one-dimensional finite difference/finite volume schemes based on spectral error analysis," *Computers & Fluids*, vol. 140, pp. 334–346, 2016.

[6] S. Xiao and T. Belytschko, "A bridging domain method for coupling continua with molecular dynamics," *Computer methods in applied mechanics and engineering*, vol. 193, no. 17-20, pp. 1645–1669, 2004.

[7] I. N. Giannakeas, T. K. Papathanasiou, and H. Bahai, "Wave reflection and cut-off frequencies in coupled fe-peridynamic grids," *International Journal for Numerical Methods in Engineering*, vol. 120, no. 1, pp. 29–55, 2019.

[8] K. U. Ingard, *Fundamentals of waves and oscillations*. Cambridge University Press, 1988.

[9] L. Brillouin, *Wave propagation in periodic structures: electric filters and crystal lattices*. Courier Corporation, 2003.

[10] P. Delsanto, R. Schechter, H. Chaskelis, R. Mignogna, and R. Kline, "Connection machine simulation of ultrasonic wave propagation in materials. ii: the two-dimensional case," *Wave Motion*, vol. 20, no. 4, pp. 295–314, 1994.

[11] P. Packo, T. Bielak, A. Spencer, T. Uhl, W. Staszewski, K. Worden, T. Barszcz, P. Russek, and K. Wiatr, "Numerical simulations of elastic wave propagation using graphical processing units—comparative study of high-performance computing capabilities," *Computer methods in applied mechanics and engineering*, vol. 290, pp. 98–126, 2015.

[12] M. J. Leamy, T. B. Autrusson, W. J. Staszewski, T. Uhl, and P. Packo, "Local computational strategies for predicting wave propagation in nonlinear media," in *Health Monitoring of Structural and Biological Systems 2014*, vol. 9064. International Society for Optics and Photonics, 2014, p. 90641J.

[13] M. J. Leamy, "Application of cellular automata modeling to seismic elastodynamics," *International Journal of Solids and Structures*, vol. 45, no. 17, pp. 4835–4849, 2008.

[14] S. Raorane, T. Uhl, and P. Packo, "Hybrid modeling of elastic wave propagation: Domain coupling and stability," *Structural Health Monitoring 2019*, 2019.

[15] P. Delsanto, T. Whitcombe, H. Chaskelis, and R. Mignogna, "Connection machine simulation of ultrasonic wave propagation in materials. i: the one-dimensional case," *Wave motion*, vol. 16, no. 1, pp. 65–80, 1992.

[16] P. Packo, P. Kijanka, and M. J. Leamy, "Spectral analysis of guided wave propagation in discretized domains under local interactions," *Proceedings of the Institution of Mechanical Engineers, Part C: Journal of Mechanical Engineering Science*, vol. 234, no. 3, pp. 746–769, 2020.